

# Prediction of blood supply in vestibular schwannomas using radiomics machine-learning classifiers

Xinting Wei (✉ [weixinting777@126.com](mailto:weixinting777@126.com))

Zhengzhou University First Affiliated Hospital <https://orcid.org/0000-0002-0482-2402>

Dixiang Song

Zhengzhou University First Affiliated Hospital

Yixuan Zhai

Zhengzhou University First Affiliated Hospital

Xiaogang Tao

Zhengzhou University First Affiliated Hospital

Chao Zhao

Zhengzhou University First Affiliated Hospital

Minkai Wang

Zhengzhou University First Affiliated Hospital

---

## Research Article

**Keywords:** acoustic neuroma, vestibular schwannoma, radiomics, machine-learning, blood supply

**Posted Date:** February 10th, 2021

**DOI:** <https://doi.org/10.21203/rs.3.rs-210542/v1>

**License:** © ⓘ This work is licensed under a Creative Commons Attribution 4.0 International License.

[Read Full License](#)

---

# Abstract

## Objective

This study attempts to explore the radiomics-based features of multi-parametric magnetic resonance imaging (MRI) and construct a machine-learning model to predict the blood supply in vestibular schwannoma preoperatively.

## Methods

By retrospectively collecting the preoperative MRI data of patients with vestibular schwannoma, patients were divided into poor and rich blood supply group according to the intraoperative recording. Patients were divided into training and test cohorts (2:1), randomly. Stable features were retained by intra-group correlation coefficients (ICCs). Four feature selection methods and four classification methods were evaluated to construct favorable radiomic classifiers. The mean area under the curve (AUC) obtained in the test set for different combinations of feature selecting methods and classifiers was calculated separately to compare the performance of the models. Obtain and compare the best combination result with the performance of differentiation through visual observation in clinical diagnosis.

## Results

191 patients were included in this study, with 119 in the rich blood supply group and 72 in the poor blood supply group. A total of 5226 features were extracted each patient, of which 3918 features were stable. LASSO and logistic regression model was selected as the optimal combinations after comparing the AUC calculated by models, which predicted the blood supply of vestibular schwannoma by K-Fold cross-validation method with a mean AUC = 0.90 and F1-score = 0.89, and the model outperformed the neurosurgeons' visual observation with a mean F1-score = 0.64.

## Conclusion

Radiomics machine-learning classifiers can accurately predict the blood supply of vestibular schwannoma by preoperative MRI data.

## Introduction

Vestibular schwannomas (VS) or Acoustic neuroma are benign nerve sheath tumors arising from Schwann cells of the acoustic nerve, comprise about 80% of cerebellopontine angle (CPA) tumors [1-3]. The annual incidence of VS is 0.6-0.8 per 100,000 people[4]. The blood supply of VS is an important factor affecting the difficulty of surgery. Previous studies have reported on Hypervascular Vestibular Schwannomas[5-8], and several studies have shown that an abundant blood supply is significantly

leading to an occurrence of facial impairment [9] and decrease of rate of resection[8]. The current method of preoperative assessment of the blood supply in VS is mainly by visual identification of the anatomical presentation of MRI and the degree of signal enhancement on T1-CE sequences. Empirically, the higher signal of the tumor on T1-CE sequences, the finding of multiple flow voids on the tumor surface or in the tumor parenchyma, and solid tumors with less cystic[8,5,6] suggest a rich blood supply to the tumor. In clinical practice, however, this method usually does not provide a satisfactory accuracy rate. Radiomics is considered to be a promising method of analyzing medical images[10], which can be combined with machine-learning methods to guide the clinic by building predictive models. The main purpose of this study is to mine the radiomics features from preoperative multi-parametric MRI of patients with VS and build a machine-learning model to predict the blood supply of VS.

## **Clinical Materials And Methods**

### **Patients**

In this research we retrospectively collected a total of 191 patients who received surgery and were diagnosed with primary VS in the First Affiliated Hospital of Zhengzhou University between December 2013 and August 2020. All patients underwent a preoperative plain and gadolinium-enhanced MRI in our center, the MRI sequences were collected including T1-weighted images, T2-weighted images, T2-weighted-Fluid-Attenuated Inversion Recovery (T2-FLAIR) images, and T1-weighted gadolinium-enhanced (T1-CE) images. Tumors in Stage I (tumor confined to the internal auditory canal, diameter 1-10mm) by Koos classification[11] were excluded because the blood supply of such small tumors may be difficult to define through the evaluation criteria of this study, and there was a possibility that insufficient radiomics information could be extracted. All surgical procedures were performed by the same highly qualified neurosurgeon. Patients were placed in a lateral position under general anesthesia during the whole procedure. All procedures were performed via a suboccipital retrosigmoid approach, and after revealing the sigmoid sinus and transverse sinus, the cerebrospinal fluid was fully released and the tumor was resected in pieces under the microscope. The blood supply of the tumor was recorded and confirmed by the senior neurosurgeon and the assistant together. Those who had less bleeding during tumor resection, the bleeding was easily removed by an aspirator, and the field under the microscope could always be kept clean, were recorded as poor blood supply; those who had more bleeding during tumor resection, and the blood in the field under the microscope was difficult to remove completely by using only one set of aspirator, were recorded as rich blood supply. The amount of intraoperative bleeding, which estimated by neurosurgeon at the end of the surgery, was also recorded to assess the reliability of the grouping.

### **MRI data acquisition**

MRI was performed with a MAGNETOM Skyra 3.0T scanner (Siemens Medical Solutions, Erlangen, Germany) and standard head coil. The imaging sequences in our study included: axial T1-CE (repetition time, 434 ms; echo time, 2.5 ms; slice thickness, 5 mm) with gadopentetate dimeglumine (Magnevist, Bayer Healthcare) was administered by injection through a peripheral venous catheter at a dose of 0.2

mmol/kg, axial T1 data (repetition time, 434 ms; echo time, 2.5 ms; slice thickness, 5 mm), Axial T2 data (repetition time, 434 ms; echo time, 2.5 ms; slice thickness, 5 mm), and axial T2-Flair data (repetition time, 434 ms; echo time, 2.5 ms; slice thickness, 5 mm). Fig. 1 shows the radiomics workflow in this study.

### **Imaging preprocessing and ROI segmentation**

The preprocessing started with the registration (brain) module of the 3D-Slicer program (version 4.11.0, Windows 64bit) to co-registration T1WI, T2WI, and T2-Flair to the T1-CE sequence (Percentage Of Samples 0.002, B-spline Grid Size 14, 10, 12), and the image correction was performed by the N4ITK MRI field bias correction module with (1,1,1) B-spline grid resolution as the confusion matrix. Next, the pyradiomics package was applied in Python environment to perform Image Normalization (normalizeScale = 100), and resampling the image (ResamplePixelSpacing = [3, 3, 3], Interpolator = sitkBSpline).

The region of interest (ROI) was drawn on T1-CE separately by two neurosurgeons with over 5 years of clinical experience using 3D-Slicer software. Neurosurgeon-A drew all ROIs manually; and Neurosurgeon B applied the Nvidia AI-Assisted Annotation (Nvidia AIAA) segmentation module[12] to semi-automatically draw ROIs by placing boundary-points and manually correct misdraw.

### **Radiomic feature extraction**

Feature extraction was performed with the python pyradiomics package, using the 8 Filter Classes built into the package, including Original, Wavelet, LoG (sigma [3.0, 5.0]), Square, SquareRoot, Logarithm, Exponential, and Gradient, using 7 feature classes, including First Order Statistics, Shape-based (3D), Shape-based (2D), Glcm: Gray Level Cooccurrence Matrix, Grlm: Gray Level Run Length Matrix, Glszm: Gray Level Size Zone Matrix, Gldm: Gray Level Dependence Matrix, and using the ROI drawn by each of doctors A and B as masks to obtain two sets of feature for A and B, respectively.

### **Feature selection**

The intraclass correlation coefficient (ICC) of feature sets A and B was calculated using the Pingouin package in Python, and only features with high stability (ICC > 0.8) were retained. To minimize human factors, we selected feature set B (ROI drawn by semi-automatic method) to proceed to the next step of feature selection. Feature selection was performed using 4 methods: student t-test, Least Absolute Shrinkage and Selection Sperator (LASSO), ANOVA, and t-test + LASSO. The optimal  $\lambda$  value in LASSO was automatically selected by bootstrap methods.

### **Feature classification and model validation**

The radiomic features selected by different methods were used to establish the model by the scikit-learn package (Version 0.23.0)[13] in python by entering them into Multivariable Linear Regression model (MLR), Support Vector Machines (SVM), Random Forest (RF), and Tree Models, respectively. The 5-repeats-3-fold cross-validation method was used, which divided the case samples into the training set

and validation set at the ratio of 2:1, and repeated the validation 5 times to obtain a total of 15 predictions results from each, and plotted the receiver operating characteristic curve (ROC) graphs of cross-validation for different feature selection methods and classifier combinations of validation sets respectively, and calculated their average area under curve (AUC). The best combination was selected by its performance (AUC). The accuracy, sensitivity, and F1-score, which considered both accuracy and sensitivity of the best model, were also calculated.

### **Artificial judgment**

Artificial judgment was performed by two other neurosurgeons with over 5 years of clinical experience, they were blinded to the intraoperative recording, and MRI image features of both cohorts were identified by visual observation. Higher signal of the tumor on T1-CE sequences, the finding of multiple flow voids on the tumor surface or in the tumor parenchyma, and solid tumors with less cystic, marked the tumor prediction as rich in blood supply. Lower signal of the tumor on T1-CE sequences, no finding of obvious flow voids related to the tumor, and tumors with multiple cystic, marked the tumor prediction as poor in blood supply. The prediction results of two neurosurgeons were recorded and compared with the gold standard (intraoperative record), and the accuracy, sensitivity, and F1-score were calculated and compared with the prediction results of the machine-learning model.

### **Statistical analysis**

The statistical analysis of baseline data was performed using IBM SPSS Statistics 21. The quantitative data was analyzed using Student's t-test, and the qualitative data was analyzed using Pearson's Chi-square test, p-value < 0.05 was considered as statistical significance.

## **Results**

### **Baseline data**

Of 191 patients, there were 109 females and 82 males, aged from 20 to 82 years, with an average age of 50.0 years (SD = 12.1). Referring to the intraoperative records, 119 patients were assigned to the rich blood supply group, and 72 patients were assigned to the poor blood supply group. Patient baseline characteristics between the poor blood supply group and the rich blood supply group are shown in Table 1. The sex and age between the two groups showed no significant statistical difference ( $p > 0.05$ ). The amount of intraoperative bleeding showed a statistically significant difference ( $p < 0.05$ ) between the two groups with a mean of 165.3 ml (SD = 156.6) in the poor blood supply group and 251.9 ml (SD = 217.9) in the rich blood supply group.

### **Feature extraction**

Each case extracted 1314 features per sequence, and 4 sequences totaled 5256 features. Excluding 10 parametric features per sequence, and computed by filters, we extracted 100 original features per sequence, 172 features in log filter, 688 features in wavelet filter, 86 features in square filter, 86 features in

squareroot filter, and 86 features in exponential filter, 86 features in logarithm filter, and 86 features in exponential filter. Computed by image types, we extracted a total of 24 shape features, 757 firstorder features, 984 glcm features, 756 glrlm features, 698 glszm features, and 664 gldm features.

### **Feature stability analysis**

After the ICCs were calculated, 3918 features with high stability ( $ICC > 0.8$ ) were retained for the next step of the feature selection process, and features with low stability ( $ICC < 0.8$ ) were excluded.

### **Feature selection and classification**

4 feature selection methods were combined with 4 classifiers, and a total of 16 combinations were applied. Table 2 shows the number of features extracted by different feature selection methods and their average AUC with different classifier combinations. LASSO had the best performance among the 4 feature selection methods, with an average AUC=0.77 for its extracted features input to the 4 classifiers. The MLR classifier had the best performance among the 4 classifiers, with an average AUC=0.76 for the 4 feature selection methods input to MLR for prediction. LASSO and MLR were selected as the best combination. Fig. 2 shows the performance of this combination in 5-repeats-3-fold validations by ROC curves and the difference in the performance of the 4 classifiers when LASSO is used as the feature selection method.

In LASSO feature selection, the optimal  $\lambda = 0.02947$  was selected from the bootstrap method, and 41 radiomic features with non-zero coefficients were retained. The selected features and their coefficient weights in LASSO are reflected in Table 3. Excluding parametric features, there were 40 selected features which had been, and they were: 22 wavelet filter features, 6 square filter features, 3 log filter features, 1 squareroot filter features, 2 logarithm filter features and 6 exponential filter feature when classified by filter; 9 firstorder features, 10 glcm features, 4 glrlm features, 10 glszm features, and 7 gldm features when classified by image types.

### **Model Validation and estimation**

The mean of the weighted average accuracy, sensitivity, F1 score, and accuracy in the prediction of tumor blood supply condition by two neurosurgeons in visual observation was 0.67, 0.63, 0.64, and 0.63, respectively. The mean score of MLR in the 3-fold-5-repeats cross-validation of the machine-learning model was 0.802, the mean AUC was 0.90 with a 95% CI from 0.801 to 0.956, and the weighted mean precision, sensitivity, F1-score, and accuracy for predicting the rich blood supply were 0.90, 0.89, 0.89 and 0.89, respectively.

## **Discussion**

The concept of radiomics was introduced in 2012 to capture the intra-tumoural heterogeneity in a non-invasive way[14], which provided clinicians with an easily accessible and low-cost means of mining the patient's imaging data for radiomic features that cannot be identified by visual observation, and applied

artificial intelligence, machine-learning, or statistical approaches to analyze the acquired high-throughput data to guide clinical practice[15].

During the surgery procedure, the blood supply of the VS can significantly affect the surgical operation. This is often due to untimely bleeding in hemorrhagic tumors, which makes it difficult for the operator to distinguish important local anatomical structures in the cerebellopontine angle region and makes electrocoagulation more likely to cause damage to adjacent tissue[9]. Some literature suggests a preoperative embolization for tumors with imaging data suggesting a significantly rich blood supply[16,6,17]. Furthermore, in cases with a rich blood supply, spare aspirators should be prepared and care should be taken not to allow raging bleeding to flow into the subarachnoid space, otherwise, the operator will need to devote considerable effort for hemostasis, resulting in the need for unscheduled blood transfusions or extended operation time. In clinical practice, the degree of blood supply to the tumor is assessed mainly by visual identification of anatomical features on MRI and the degree of enhancement of the tumor on T1-CE. However, the prediction by visual observation of the two neurosurgeons in this study showed that this method was not quite reliable in practice (precision=0.67, sensitivity=0.63). Therefore, it is necessary to develop a tool that can more effectively predict the blood supply of VS preoperatively. In this study, we established a reproducible model by combining a multisequence radiomics method with a machine-learning classifier through repeated sampling and cross-validation, which can preoperatively predict the blood supply of VS more accurately. By comparing, the machine-learning model has a significantly better performance than the visual observation in terms of judgment. Our model holds promise for providing surgeons with additional information during preoperative evaluation, such as better assessment of the required operation duration to improve anesthesia; adequate preparation of blood transfusion or autologous blood transfusion, and multiple sets of suction for backup in the operative field preoperatively for tumors with rich blood supply.

In the selection of patient MRI sequences, we included T1-CE as the background for drawing the ROI because most of the VS had significant enhancement on T1-CE[18,19], and the boundary of the tumor could be clearly outlined. To obtain more voxels, we extracted the T1WI, T2WI, and T2-Flair sequences which were commonly used in the diagnosis of VS, and aligned them to the drawn ROI in T1-CE for co-registration[20,19]. The ADC sequence proved to be valuable in applications such as differential diagnosis, treatment response prediction, and prognostic judgment of VS[21,22], especially in the determination of cystic and solidity in VS[23], so we initially included it in the study. However, the co-registration of ADC to T1-CE sequences was always unsatisfactory in terms of anatomical image correspondence, probably due to the distorted and uneven data caused by adjacent structures and inhomogeneous internal structures of the lesion[23], which may lead to an increase in confounding factors and a potential decrease in reproducibility[24]. Giordano M et al. applied multiple ROIs to reduce structural inhomogeneity of the lesion, but the workload of this method was too large, so we finally discarded the ADC sequences.

To obtain a model with better performance, we chose several feature selection methods and classifiers commonly used in the current medical context for combination and finally selected LASSO for feature

selection and MLR for modeling based on AUC. As we can see from Table 2, LASSO has significantly higher reliability than other feature filtering methods, and this method has been widely used for high-dimensional data processing[25], where the coefficients of unimportant features are compressed to zero by a penalty algorithm to achieve dimensionality reduction of the data. The performance of both MLR and SVM classifiers in our results is satisfactory (0.90 vs. 0.85), and both are applicable in medium-sized samples, with MLR demonstrating better performance in this study probably because it usually performs well on binary data.

The discussion of the transition of radiomics to practical clinical applications has always been a critical issue, and one of the most important aspects of this process is the reproducibility of the acquisition of radiomics features. To reduce the variation among cases in the MRI cases and among different sequences of the same case, we performed the same preprocessing of all the images, including co-registration, correction, normalization, and resampling with same parameters. To minimize human variation, we drew ROIs by two neurosurgeons using different methods and analyzed the extracted radiomics features of both groups for ICC, and excluded those features that differed significantly among groups. However, these basic processes do not necessarily guarantee practical applications. Schwier M et al. pointed out that the type of image, pre-processing and ROIs used to evaluate features can significantly change the repeatability of certain features, so the recommended practice is to publish the details of processing and parameter configuration as much as possible[26]. Therefore, on this basis, we published as much detail as possible in the whole operation. The yaml file used in the feature extraction process and the MLR model constructed in the feature classification process in this study are available on Supplemental material 1 and Supplemental material 2.

The determination of the actual blood supply classification relied mainly on surgeons' intraoperative assessment, though subjective errors were inevitable, we standardized the criteria as much as possible within our medical team, and some cases that were difficult to distinguish or whose descriptions were ambiguous when the blood supply was recorded intraoperatively were excluded from this study. We collected and analyzed the intraoperative blood loss of patients, and in our statistics we found that intraoperative bleeding could not be used as a basis for classification of blood supply. However, the results showed a statistical difference between the two groups in terms of intraoperative blood loss when relying on surgeon's intraoperative assessment for grouping, which to some extent reflects the reliability of the grouping. Besides, we collected hemoglobin concentrations from each patient during the perioperative period at 6:00 p.m. preoperatively on the day of surgery and at 6:00 p.m. postoperatively on the day following surgery, and no statistical or practical significance was found in the analysis. Previous studies have shown that methods relying on perioperative blood indicators or calculating the volume of suction fluid are inaccurate for calculating perioperative blood loss[27-29], which may also support the negative results of our analysis of perioperative hemoglobin concentration changes. A feasible method of quantification is to calculate total intraoperative hemoglobin by measuring the hemoglobin concentration and fluid volume of the suction fluid, and this method is costly but relatively reliable and can be used as a method to further improve related studies.

# Conclusion

The radiomics machine-learning classifiers is an effective method to predict the blood supply of vestibular schwannoma by preoperative MRI data, which has a better performance than neurosurgeons' judgment by visual observation of MRI image and can provide more information for surgeons to help neurosurgeons make operative strategy

# Declarations

**Funding** No funding was received for this research.

**Conflicts of interest/Competing interests** The authors declare that there is no conflict of interest or competing interests.

**Availability of data and material** The datasets used or analysed during the current study are available from the corresponding author on reasonable request.

**Code availability** The code used or analysed during the current study are available from the corresponding author on reasonable request.

**Authors' contributions** DS: conception, manuscript writing, and data analysis. YZ: Programming and critical review. MW and CZ: data acquisition. XW: conception and critical review. All authors proofread and approved the manuscript.

**Ethics approval** Approval of the Ethical Committee of the Institute was taken for this retrospective study.

**Consent to participate** Not applicable

**Consent for publication** Not applicable

# Acknowledgments

The authors would like to acknowledge Dr. Li, who shared his acknowledgment on public video-sharing platform selflessly.

# References

1. Mahaley M, Mettlin C, Natarajan N, Laws E, Peace B (1990) Analysis of patterns of care of brain tumor patients in the United States: a study of the Brain Tumor Section of the AANS and the CNS and the Commission on Cancer of the ACS. *Clinical neurosurgery* 36:347-352
2. Reznitsky M, Petersen MMBS, West N, Stangerup S-E, Caye-Thomasen P (2020) The natural history of Vestibular Schwannoma growth-prospective 40-year data from an unselected national cohort. *Neuro-oncology*

3. Halliday J, Rutherford SA, McCabe MG, Evans DG (2018) An update on the diagnosis and treatment of vestibular schwannoma. *Expert Review of Neurotherapeutics* 18 (1):29-39
4. Alfaifi A, AlMutairi O, Allhaidan M, Alsaleh S, Aylan A (2018) The Top 50 Most-Cited Articles on Acoustic Neuroma. *World Neurosurg* 111:e454-e464. doi:10.1016/j.wneu.2017.12.090". <https://doi.org/10.1016/j.wneu.2017.12.090>"
5. Yamakami I, Kobayashi E, Iwadata Y, Saeki N, Yamaura A (2002) Hypervascular vestibular schwannomas. *Surgical neurology* 57 (2):105-112
6. LeMay DR, Sun JK, Fishback D, Locke GE, Giannotta SL (1998) Hypervascular acoustic neuroma. *Neurol Res* 20 (8):748-750. doi:10.1080/01616412.1998.11740595". <https://doi.org/10.1080/01616412.1998.11740595>"
7. Bonneville F, Cattin F, Czorny A, Bonneville J (2002) Hypervascular intracisternal acoustic neuroma. *Journal of neuroradiology Journal de neuroradiologie* 29 (2):128-131
8. Teranishi Y, Kohno M, Sora S, Sato H, Nagata O (2018) Hypervascular vestibular schwannomas: Clinical characteristics, angiographical classification, and surgical considerations. *Operative Neurosurgery* 15 (3):251-261
9. Talfer S, Dutertre G, Conessa C, Desgeorges M, Poncet J-L (2010) Surgical treatment of large vestibular schwannomas (stages III and IV). *European Annals of Otorhinolaryngology, Head and Neck Diseases* 127 (2):63-69
10. Aerts HJ (2016) The potential of radiomic-based phenotyping in precision medicine: a review. *JAMA oncology* 2 (12):1636-1642
11. Koos WT, Böck F, Ammerman B, Spetzler RF (1976) *Clinical microneurosurgery*. Thieme,
12. Sachidanand Alle, Yuan-Ting Hsieh, Andras Lasso, Steve Piper, anfang, Biggs. S (2019) Nvidia AI-assisted annotation (AIAA) for 3D Slicer. <https://github.com/NVIDIA/ai-assisted-annotation-client>.
13. Abraham A, Pedregosa F, Eickenberg M, Gervais P, Mueller A, Kossaifi J, Gramfort A, Thirion B, Varoquaux G (2014) Machine learning for neuroimaging with scikit-learn. *Frontiers in neuroinformatics* 8:14
14. Lambin P, Rios-Velazquez E, Leijenaar R, Carvalho S, van Stiphout RG, Granton P, Zegers CM, Gillies R, Boellard R, Dekker A, Aerts HJ (2012) Radiomics: extracting more information from medical images using advanced feature analysis. *Eur J Cancer* 48 (4):441-446. doi:10.1016/j.ejca.2011.11.036". <https://doi.org/10.1016/j.ejca.2011.11.036>"
15. Gillies RJ, Kinahan PE, Hricak H (2016) Radiomics: Images Are More than Pictures, They Are Data. *Radiology* 278 (2):563-577. doi:10.1148/radiol.2015151169". <https://doi.org/10.1148/radiol.2015151169>"
16. Perneczky A (1980) Blood supply of acoustic neurinomas. *Acta neurochirurgica* 52 (3-4):209-218
17. Rushworth RG, Sorby WA, Smith SF (1984) Acoustic neuroma in a child treated with the aid of preoperative arterial embolization: Case report. *Journal of neurosurgery* 61 (2):396-398

18. AHMAD TT, Kanwal N, Ameer S, Nasir S (2014) Diagnostic accuracy of magnetic resonance imaging in detection of acoustic neuroma. *Biomedica* 30 (1):5
19. Robson A, Leighton S, Anslow P, Milford C (1993) MRI as a single screening procedure for acoustic neuroma: a cost effective protocol. *Journal of the Royal Society of Medicine* 86 (8):455
20. Curati W, Graif M, Kingsley D, King T, Scholtz C, Steiner R (1986) MRI in acoustic neuroma: a review of 35 patients. *Neuroradiology* 28 (3):208-214
21. Kunigelis KE, Hosokawa P, Arnone G, Raban D, Starr A, Gurau A, Sunshine A, Bunn J, Thaker AA, Youssef AS (2020) The predictive value of preoperative apparent diffusion coefficient (ADC) for facial nerve outcomes after vestibular schwannoma resection: clinical study. *Acta Neurochirurgica*
22. Camargo A, Schneider T, Liu L, Pakpoor J, Kleinberg L, Yousem DM (2017) Pretreatment ADC values predict response to radiosurgery in vestibular schwannomas. *American Journal of Neuroradiology* 38 (6):1200-1205
23. Giordano M, Samii A, Samii M, Nabavi A (2019) Magnetic Resonance Imaging-Apparent Diffusion Coefficient Assessment of Vestibular Schwannomas: Systematic Approach, Methodology, and Pitfalls. *World Neurosurg* 125:e820-e823. doi:10.1016/j.wneu.2019.01.176". <https://doi.org/10.1016/j.wneu.2019.01.176>"
24. Shiri I, Hajianfar G, Sohrabi A, Abdollahi H, P. Shayesteh S, Geramifar P, Zaidi H, Oveisi M, Rahmim A (2020) Repeatability of radiomic features in magnetic resonance imaging of glioblastoma: Test-retest and image registration analyses. *Medical Physics* 47 (9):4265-4280
25. Fonti V, Belitser E (2017) Feature selection using lasso. *VU Amsterdam Research Paper in Business Analytics* 30:1-25
26. Schwier M, van Griethuysen J, Vangel MG, Pieper S, Peled S, Tempany C, Aerts H, Kikinis R, Fennessy FM, Fedorov A (2019) Repeatability of Multiparametric Prostate MRI Radiomics Features. *Sci Rep* 9 (1):9441. doi:10.1038/s41598-019-45766-z". <https://doi.org/10.1038/s41598-019-45766-z>"
27. Johar RS, Smith RP (1993) Assessing gravimetric estimation of intraoperative blood loss. *J Gynecol Surg* 9 (3):151-154. doi:10.1089/gyn.1993.9.151". <https://doi.org/10.1089/gyn.1993.9.151>"
28. Guinn NR, Broomer BW, White W, Richardson W, Hill SE (2013) Comparison of visually estimated blood loss with direct hemoglobin measurement in multilevel spine surgery. *Transfusion* 53 (11):2790-2794. doi:10.1111/trf.12119". <https://doi.org/10.1111/trf.12119>"
29. Stahl DL, Groeben H, Kroepfl D, Gautam S, Eikermann M (2012) Development and validation of a novel tool to estimate peri-operative blood loss. *Anaesthesia* 67 (5):479-486. doi:10.1111/j.1365-2044.2011.06916.x". <https://doi.org/10.1111/j.1365-2044.2011.06916.x>"

## Tables

Table 1 Sex, age and intraoperative bleeding distribution between the poor blood supply group and the rich blood supply group

Characteristics		Groups		Total	p-value
		Poor blood supply	Rich blood supply		
Sex	Male	26	56	72	0.09
	Female	46	63	109	
Age (y)		52.7 ± 11.8	48.4 ± 12.0	50.0 ± 12.1	0.73
Intraoperative bleeding (ml)		165.3 ± 156.6	251.9 ± 217.9	219.0 ± 201.2	0.01

(mean ± standard deviation)

Table 2 Number of features extracted by different feature extraction methods and the average AUC

Feature_Selection_Methods	AUC of Classification Methods					Number of selected Voxel
	RF	MLR	SVM	DT	average	
t_test	0.70	0.73	0.72	0.66	0.70	28
LASSO	0.72	0.90	0.85	0.61	0.77	41
ANOVA	0.60	0.61	0.50	0.61	0.58	14
t_test + LASSO	0.73	0.80	0.64	0.66	0.71	25
average	0.69	0.76	0.71	0.63	0.70	

Table 3 Selected features and their coefficient weights in LASSO feature selection method

Sequences	Features	Coefficient
T1-CE	diagnostics_Image-original_Maximum	0.024008
	wavelet-HLL_gldm_DependenceVariance	-0.055243
	wavelet-HLH_glszm_LargeAreaHighGrayLevelEmphasis	-0.011757
	wavelet-HLH_gldm_DependenceVariance	-0.028858
	wavelet-HHL_firstorder_Kurtosis	0.097581
	wavelet-HHH_glcm_JointAverage	0.005772
	wavelet-HHH_glrIm_RunEntropy	0.016309
	wavelet-HHH_glszm_GrayLevelNonUniformityNormalized	-0.022407
	square_glcm_JointEnergy	0.033220
	square_glcm_InverseVariance	-0.050472
	squareroot_glszm_SizeZoneNonUniformityNormalized	-0.051366
	logarithm_firstorder_InterquartileRange	0.014329
	exponential_glszm_SizeZoneNonUniformity	0.003370
	T1WI	wavelet-LHL_firstorder_Range
wavelet-LHL_glszm_LargeAreaHighGrayLevelEmphasis		-0.006220
wavelet-HLL_firstorder_90Percentile		0.008324
wavelet-HLL_glrIm_GrayLevelNonUniformityNormalized		-0.029011
wavelet-HLL_glszm_GrayLevelNonUniformityNormalized		-0.008792
wavelet-HLH_gldm_DependenceVariance		0.025165
wavelet-HHL_firstorder_Minimum		-0.024770
square_glszm_GrayLevelNonUniformityNormalized		-0.009218
exponential_glcm_Idmn		-0.012293
T2WI	log-sigma-3-0-mm-3D_glrIm_LongRunHighGrayLevelEmphasis	-0.031169
	log-sigma-3-0-mm-3D_glszm_LargeAreaHighGrayLevelEmphasis	-0.020605
	wavelet-HHH_glcm_Autocorrelation	0.004800
	wavelet-HHH_gldm_LargeDependenceLowGrayLevelEmphasis	0.002890
	square_glcm_Imc2	-0.023028
	exponential_glcm_ClusterProminence	0.036161

	exponential_glrIm_ShortRunLowGrayLevelEmphasis	0.064972
	exponential_gldm_DependenceVariance	0.050860
	Flair_log-sigma-3-0-mm-3D_firstorder_InterquartileRange	-0.029460
	Flair_wavelet-LLH_gldm_LargeDependenceHighGrayLevelEmphasis	0.004585
T2-FLAIR	wavelet-LHH_glcm_ClusterShade	0.009670
	wavelet-LHH_glszm_LowGrayLevelZoneEmphasis	0.012365
	wavelet-HLH_firstorder_Maximum	-0.019111
	wavelet-HHL_firstorder_Maximum	0.008752
	wavelet-HHH_firstorder_RobustMeanAbsoluteDeviation	-0.018533
	square_glcm_ClusterShade	0.012879
	square_glszm_ZoneVariance	-0.006836
	logarithm_glcm_ClusterShade	0.035088
	exponential_gldm_DependenceVariance	0.017067

## Figures

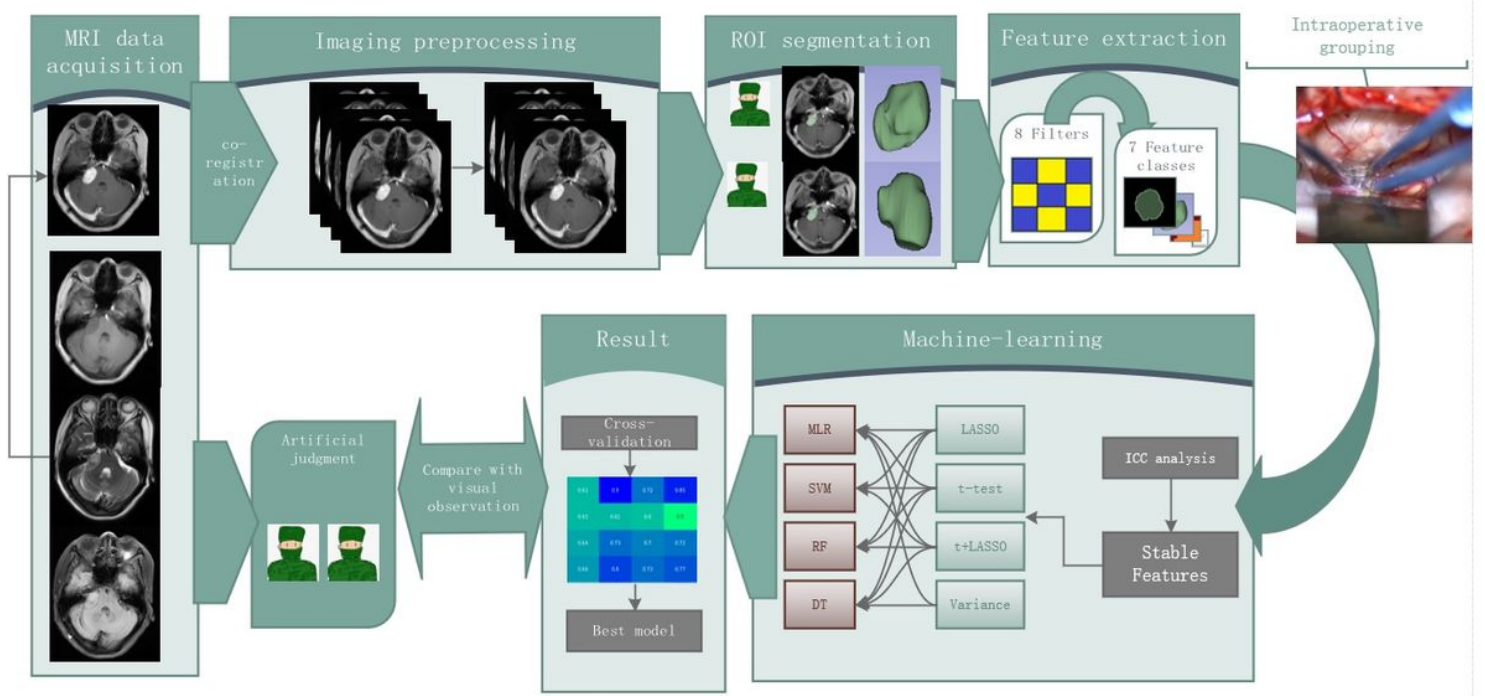
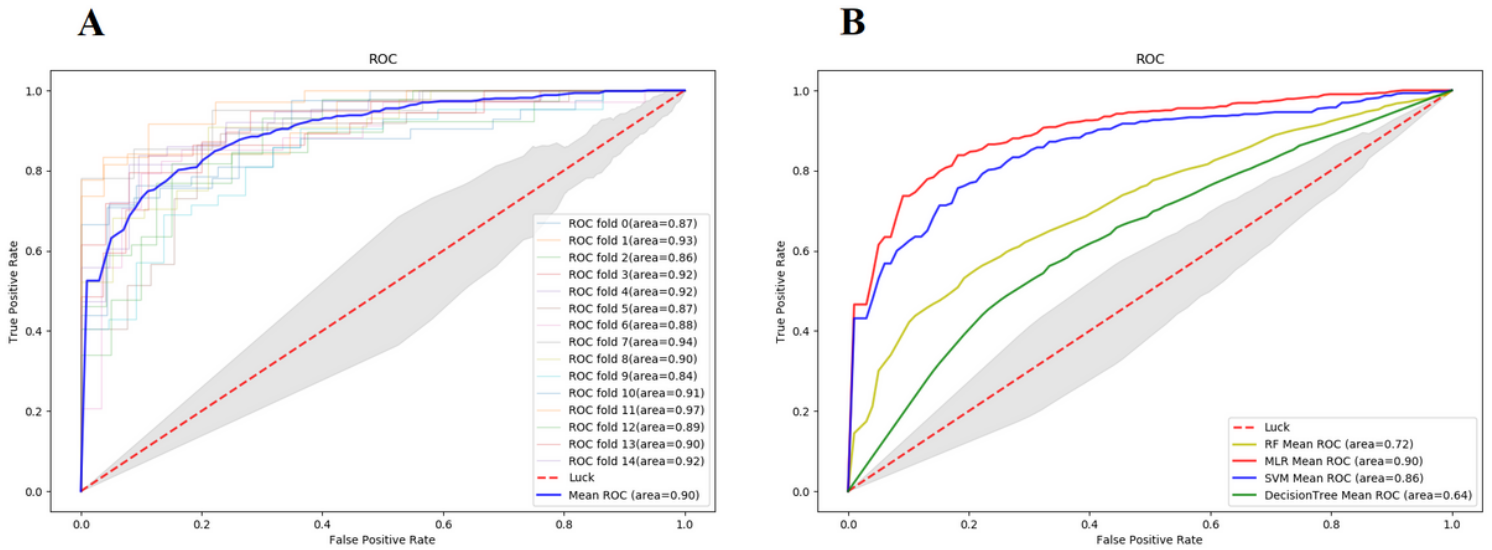


Figure 1

The radiomics workflow in this study.



**Figure 2**

The performance of this combination in 5-repeats-3-fold validations by ROC curves and the difference in the performance of the 4 classifiers when LASSO is used as the feature selection method.

## Supplementary Files

This is a list of supplementary files associated with this preprint. Click to download.

- [Supplementalmaterial1.yaml](#)
- [Supplementalmaterial2.model](#)